J. of Supercritical Fluids 152 (2019) 104571

Contents lists available at ScienceDirect

The Journal of Supercritical Fluids

journal homepage: www.elsevier.com/locate/supflu

Investigation of the effect of gel properties on supercritical drying kinetics of ionotropic alginate gel particles

İbrahim Şahin[a], Erdal Uzunlar[b], Can Erkey[a,*]

[a] Department of Chemical and Biological Engineering, Koç University, Rumelifeneri Yolu, Sarıyer, 34450, İstanbul, Turkey
[b] Department of Chemical Engineering, İzmir Institute of Technology, Gülbahçe Mah., Urla, 35430, İzmir, Turkey

HIGHLIGHTS

- Kinetics of supercritical drying of a series of ionotropic alginate gel particles was investigated.
- Supercritical drying kinetics was predicted using a mathematical model.
- Changes in drying kinetics could be accounted by changes in particle diameter and porosity.
- Gel particles of diameter of 4.5 mm could be supercritically dried in less than 25 min.

GRAPHICAL ABSTRACT

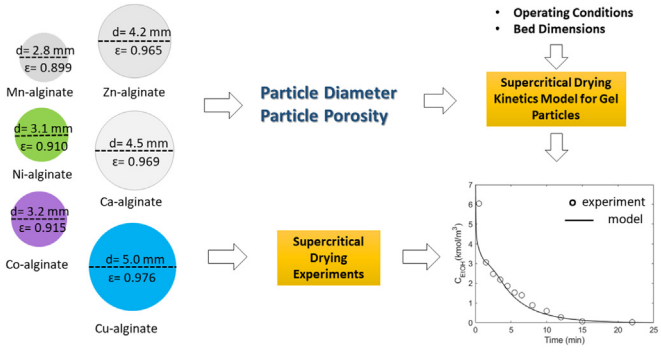

ARTICLE INFO

Article history:
Received 15 December 2018
Received in revised form 19 June 2019
Accepted 10 July 2019
Available online 11 July 2019

Keywords:
Supercritical drying
Kinetics
Alginate
Mass transfer coefficient
Mathematical model
Aerogel

ABSTRACT

A series of spherical ionotropic alginate gel particles with different diameters ranging from 2.8 mm to 5.0 mm and porosities ranging from 0.899 to 0.976 were prepared by dripping a Na-alginate solution into a solution of salts of divalent cations (Ca^{2+}, Mn^{2+}, Ni^{2+}, Co^{2+}, Cu^{2+} and Zn^{2+}). After solvent exchange with ethanol, kinetics of supercritical drying of these ionotropic alginate gel particles in a packed bed was investigated at 308–338 K and 100–120 bar. Experimental data were compared with predictions of a model which considers diffusive transport inside the pores and convection in the flowing fluid stream. The model predicted drying profiles by taking into account only the changes in porosity and diameter of the gel particles. A convective mass transfer coefficient correlation that was originally developed for supercritical drying of Ca-alginate gel particles was found to be suitable for M-alginate gel particles.

1. Introduction

Aerogels are mesoporous materials that have low density, high porosity and high pore volume. Aerogels can be organic or inorganic and can be produced as monoliths, fibers and particles. Significant research efforts have been exhausted in many laboratories around the world for development of monolithic transparent silica aerogels in the form of panels and silica aerogel based blankets for the past three decades [1–6]. Recently, a wide variety of organic and inorganic aerogels and their composites in the form of particles have been under investigation for various applications such as adsorption, catalysis, energy, sensing, cosmetics and food [7–10]. In some cases, the unique and tunable properties of aerogel particles has led to very promising results [11]. Aerogel particles are obtained

* Corresponding author.
E-mail address: cerkey@ku.edu.tr (C. Erkey).

https://doi.org/10.1016/j.supflu.2019.104571
0896-8446/

by supercritical extraction of solvent (supercritical drying) from gel particles which can be produced by a number of methods such as emulsion gelation (with and without surfactant) and dripping [7].

In supercritical drying, a supercritical fluid, generally supercritical CO_2 ($scCO_2$), is continuously passed over gel particles that are packed in a bed until the solvent is completely removed from the pores of the gel particles. During this process, solvent inside the pores of the gel is transported by diffusion to the surface of the gel particles owing to the presence of a concentration gradient. The solvent is then transported by convective mass transfer from the surface of the gel particles into the flowing fluid stream. An understanding of the kinetics of supercritical drying of gel particles is important not only for the design and optimization of large scale supercritical dryers but also for improving our understanding of transport processes in supercritical fluids.

There has been a limited number of experimental and theoretical studies on kinetics of supercritical drying of gel particles [12]. Selmer et al. developed a model for predicting the kinetics of supercritical drying in a bed packed with spherical silica alcogel particles [13]. The differential mass balance equations were written separately for ethanol in the fluid phase in the alcogel and for ethanol in the fluid phase flowing around the gel particles. The mass transfer of the solvent in the alcogel was considered as a diffusive process described by Fick's second law with the use of an effective diffusion coefficient. A partial differential equation was written to describe the variation of ethanol concentration in the flowing fluid as a function of time and bed height which included a convective term due to the flowing fluid, a term for the convective mass transfer of ethanol from the surface of the gel particle to the flowing fluid and an axial dispersion term due to diffusion of ethanol in the flowing fluid stream around the particles. The solution of these coupled partial differential equations by using proper initial and boundary conditions yielded concentration profiles of ethanol inside the particle and along the height of the packed bed. The model was then used to simulate the effects of various parameters such as operating conditions, flow rate, particle size, and bed dimensions on drying times. The mass transfer coefficient was calculated utilizing the existing correlations in the literature [13]. The simulations suggested the presence of two distinct regimes. Comparison of the model results with the experimental data for drying of spherical silica alcogel particles in a packed bed indicated that there was an underestimation of the drying profiles for the early phases of drying [14]. These deviations were attributed to the simplified description of the hydrodynamics in the packed bed. Simulations using the proposed model showed that staying in the diffusion-limited region near to the transition Biot number was essential to minimize the drying duration and CO_2 consumption. Both of these two studies indicated that accurate description of convective mass transport at the gel-$scCO_2$ interface is crucial for the optimization of supercritical drying of gel particles.

Usually, correlations in terms of dimensionless numbers are used to calculate convective mass transfer coefficients in supercritical fluid applications [15–20]. A Sherwood number correlation was derived for experiments carried out under supercritical conditions for the first time by Tan et al [20]. Later, modified versions of this correlation were developed and utilized in several studies concerning supercritical extraction of natural materials [15,16]. We recently modeled the drying of spherical calcium alginate alcogel particles in a packed bed using a similar model to the model developed by Selmer et al [21,22]. A correlation for predicting external mass transfer coefficients for supercritical drying of alcogel particles in a packed bed was developed for the first time by fitting the model results to experimental data. A good agreement between the experimental data and model results was achieved using this correlation.

In this study, our objective was to expand our investigation by studying the effect of gel properties on the kinetics of supercritical drying of gel particles in a packed bed. To that end, a series of spherical ionotropic alginate gel particles with different diameters and porosities were prepared by dripping a Na-alginate solution into a solution of salts of divalent cations (Ca^{2+}, Mn^{2+}, Ni^{2+}, Co^{2+}, Cu^{2+} and Zn^{2+}). Supercritical drying experiments for a bed packed with these ionotropic alginate gel particles were performed at various operating conditions. Concentration of ethanol in the flowing fluid stream at the exit of the drying vessel was measured as a function of time. Experimental data were compared with the results of the predictions of our previously developed model. The kinetic data in agreement with the model could be very helpful in the design of supercritical drying units for production of ionotropic aerogels for various applications in large scale [23–29].

2. Materials and methods

2.1. Materials

Sodium salt of alginic acid from brown algae (medium viscosity, product number: A2033 and low viscosity, product number: A1112), and calcium chloride (anhydrous granular, >93%), cobalt(II) chloride hexahydrate (Ph. Eur., 99–102%), zinc sulfate heptahydrate (Ph. Eur., 99.0–103.0%), manganese(II) chloride tetrahydrate (≥99%) were obtained from Sigma-Aldrich. Nickel(II) nitrate hexahydrate (analysis grade) and copper(II) nitrate trihydrate (analysis grade) were purchased from Merck. Ethanol (99.9% purity) was purchased from Isolab. CO_2 was obtained from Air Liquide and had a stated purity of 99.9%.

2.2. Preparation of spherical ionotropic alginate gel particles

Ionotropic alginate gel particles with Cu^{2+}, Ca^{2+}, Zn^{2+}, Co^{2+}, Ni^{2+} and Mn^{2+} ions were synthesized by dripping a 1.5 wt% aqueous alginate solution (medium viscosity) into a 0.2 M aqueous metal salt solution which was constantly stirred at 200 rpm. Formed hydrogel particles were cured in the corresponding metal salt solutions for overnight. After that, hydrogel beads were subjected to a stepwise solvent-exchange procedure with mixtures of ethanol and water for a duration of 2 h at each step (10%, 30%, 50%, 70%, 90% and 100% ethanol by vol., respectively) to prevent excessive shrinkage. The ratio of the volume of ethanol solution to the volume of the hydrogel particles were close to 2 for each solvent exchange step. Before supercritical drying, gels were kept in fresh ethanol for 24 h. Since alginate's affinity towards divalent ions vary with the type of the divalent ion (alginate affinity towards various divalent ions follows the order of Pb > Cu > Cd > Ba > Sr > Ca > Co, Ni, Zn > Mn [30,31]), obtained hydrogels after curing step had different particle diameters and porosities. The particle diameter of hydrogel particles measured after they were initially formed in the metal salt solution bath was 5.9 mm. After curing and solvent exchange, the particle diameter of alcogel particles were measured as 5.0, 4.5, 4.2, 3.2, 3.1, and 2.8 mm for Cu, Ca, Zn, Co, Ni, and Mn-alginate, respectively. Aerogels obtained after supercritical drying of these alcogels were named as "1.5M-Alg" where M stands for the metal and 1.5 stands for the concentration of the sodium alginate solution in wt. %.

Calcium alginate alcogel particles were also prepared by dripping 3 wt. %, 5 wt. % and 10 wt. % alginate solutions (low viscosity) into a 0.2 M aqueous $CaCl_2$ solution which was constantly stirred at 200 rpm. Resulting hydrogels, having an average diameter of 5.9 mm, were subjected to a stepwise solvent-exchange procedure with mixtures of ethanol and water for a duration of 2 h at each step (10%, 30%, 50%, 70%, 90% and 100% ethanol by vol., respectively) to

prevent excessive shrinkage. Before supercritical drying, gels were kept in fresh ethanol (99.9% purity) for 24 h. Aerogels obtained after supercritical drying of these alcogels were named as "XCa-Alg-Low" where X stands for the weight percent of Na-alginate solution used in preparation of the samples.

2.3. Supercritical drying of alginate alcogels with $scCO_2$

Supercritical drying of synthesized alginate alcogels was performed in an Applied Separations Speed SFE unit (tubular vessel, length = 15.94 cm, diameter = 1.43 cm, volume = 26 ml). A schematic representation of the experimental setup can be seen in Fig. 1. Details of the apparatus and the supercritical drying procedure are given elsewhere [21]. In summary, the preheated bed was packed with alginate gel particles and topped with ethanol. Subsequently, CO_2 was passed through the vessel after pressurization. The pressurization rate was very fast and close to 30 bar/s. Ethanol was collected in glass vials immersed in a dry ice - acetone bath kept at −75 °C to minimize evaporation losses of ethanol. When the amount of collected ethanol in the first vial was approximately equal to the amount of excess ethanol initially added to the vessel, the vial was replaced with an empty one. Time "zero" in experimental concentration plots refers to this time. The ethanol in the first vial was assumed to be the excess ethanol placed in the vessel. The collection time in the first vial lasted usually anywhere from 1 to 2 min which was much shorter than the duration of a typical drying experiment. Ethanol extracted from the alcogel was discretely collected in separate vials within certain time intervals and weighed. A total of 10–12 vials were used for a drying experiment. Therefore, total duration of vial changing was about 20 s which was very short compared to an average drying time of 25 min. Material balance closures for ethanol, listed in Table S1 and S2 of Supplementary Information, were better than 5% for all the experiments.

The concentration of ethanol in the effluent stream at the extraction conditions, EC, $C_{EtOH-EC}$ was calculated by dividing the mass of ethanol collected in the vial, m_{EtOH}, by the molecular weight of ethanol, $M_{w,EtOH}$, the time interval of collection, Δt, and the volumetric flow rate of the effluent stream at extraction conditions, $Q_{mixture-EC}$.

$$C_{EtOH-EC} = \frac{m_{EtOH}}{Q_{mixture-EC} \times M_{w,EtOH} \times \Delta t} \quad (1)$$

$Q_{mixture-EC}$ was calculated by adding the volumetric flow rates of ethanol, $Q_{EtOH-EC}$, and CO_2, Q_{CO2-EC}, assuming that CO_2 and ethanol formed ideal mixtures at these conditions.

$$Q_{mixture-EC} = Q_{EtOH-EC} + Q_{CO2-EC} \quad (2)$$

$Q_{EtOH-EC}$ and Q_{CO2-EC} were calculated from the experimentally determined volumetric flow rate of ethanol at standard condition ($Q_{EtOH-std} = m_{EtOH}/(\rho_{EtOH} \times \Delta t)$, where ρ_{EtOH} is the density of ethanol at standard conditions) and volumetric flow rate of CO_2 at standard conditions, $Q_{CO2-std}$ (2–4 L/min) by material balances around the micro-metering valve for ethanol and CO_2, given by:

$$Q_{EtOH-EC} = \bar{V}_{EtOH-EC} \times \frac{Q_{EtOH-std}}{\bar{V}_{EtOH-std}} \quad (3)$$

$$Q_{CO2-EC} = \bar{V}_{CO2-EC} \times \frac{Q_{CO2-std}}{\bar{V}_{CO2-std}} \quad (4)$$

where $\bar{V}_{EtOH-EC}$ and $\bar{V}_{CO2-EC}$ are molar volumes of ethanol and CO_2 at the extraction conditions, and $\bar{V}_{EtOH-std}$ and $\bar{V}_{CO2-std}$ are molar volumes of ethanol and CO_2 at standard conditions.

The shrinkage of the particle diameter of the gels after supercritical drying were only about 4% for all of the prepared samples except Cu-alginates for which an 8% shrinkage in diameter was observed.

2.4. Characterization of alginate aerogel particles

The average particle diameter, d_p, of gels was determined by measuring the diameter of at least 20 particles. The bulk density of the aerogel, ρ_{bulk}, was determined by first measuring the average mass of particles by weighing the aerogel particles using a balance and then dividing the calculated average mass to the average particle volume, which was calculated from the average particle diameter. The bed porosity was measured by filling the extraction vessel with alcogel particles and rapidly adding a sufficient amount of ethanol to fill the void volume of the bed. Then, the bed porosity was calculated by dividing the added ethanol volume to the volume of extraction vessel. At least three measurements were done for each sample.

The skeletal density of the aerogel samples was determined using a pycnometer, which was suggested for determination of the skeletal density of porous materials [32,33]. Skeletal densities of several silica aerogels were also measured by liquid pycnometry in several studies [34–36]. In our procedure, ethanol at room temperature was used as the solvent. First, aerogel particles were crushed and placed into the pycnometer and ethanol was added. A certain time was allowed to pass until trapped air inside the pores was displaced by ethanol and there were no bubbles. Sufficient amount of ethanol was then added to fully fill the pycnometer. The skeletal density of the sample was calculated using the weights of empty pycnometer, pycnometer filled with ethanol and pycnometer filled with ethanol and the sample. Following this calculation, the particle porosity of the samples was calculated as follows:

$$\varepsilon = 1 - \frac{\rho_{bulk}}{\rho_{skeletal}} \quad (5)$$

where ρ_{sketal} is the skeletal density of the aerogels and ε is the particle porosity. The total pore volume per mass of aerogel, V_p, was also calculated by using the measured densities as follows;

$$V_p = \frac{1}{\rho_{bulk}} - \frac{1}{\rho_{skeletal}} \quad (6)$$

The pore size, d_{pore}, and the Brauner, Emmet and Teller (BET) surface area, S_{BET}, of the aerogel samples were determined by N_2 adsorption using a Micromeritics ASAP 2020 instrument. N_2 adsorption/desorption isotherms were obtained with a relative pressure (P/P_0) ranging from 10^{-7} to 0.995. The desorption curve was used for the determination of average pore size. The pore volume, $V_{p,BET}$, was taken as the adsorbed volume at maximum pressure (P/P_0).

3. Results and discussions

3.1. Properties of aerogels

The physical and textural properties of the synthesized aerogels are shown in Table 1. The particle diameters of the synthesized aerogels with different cations were found relatively to be in the order of Cu > Ca > Zn > Co > Ni > Mn. This trend was observed to follow the trend of alginate's affinity towards the divalent cations. Therefore, this results indicates that alginate gels tend to shrink more when the affinity of the alginate towards the cation is weaker. On the other hand, skeletal density did not change much with the type of divalent cation.

The substantial differences between the pore volumes calculated from the particle densities and from N_2 physisorption data for all of the ionotropic aerogels can be attributed to the presence of macropores assuming that (i) all pores were accessible by N_2, (ii) the equilibration time of each adsorption and desorption step was sufficient and (iii) there was no contraction/expansion of the gel during N_2 physisorption [37]. Since the particle size of the aerogels did not

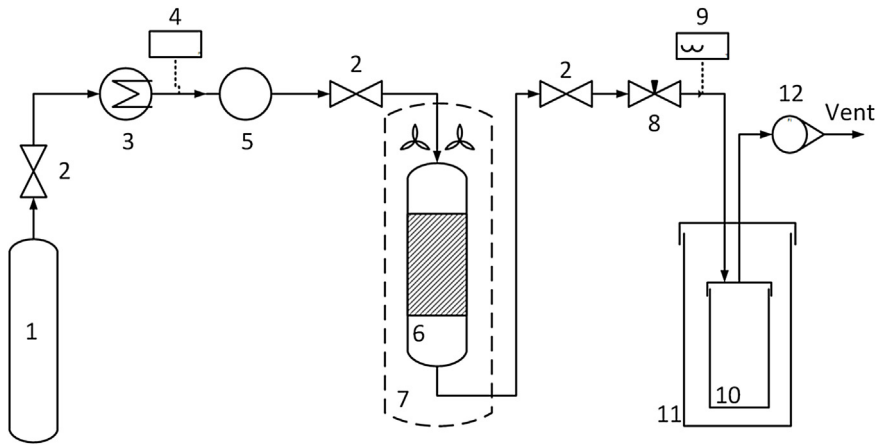

Fig. 1. Schematic diagram of experimental set-up (1. CO_2 tank, 2. Valve, 3. Cooler, 4. Pressure transducer, 5. Pump, 6. Tubular extraction vessel, 7. Oven, 8. Micro-metering Valve, 9. Thermocouple, 10. Sample collection vial, 11. Dry ice cooling bath, 12. Rotameter).

Table 1
Physical and textural properties of the prepared samples.

	d_p (mm)	ρ_{bulk} (g/cm^3)	$\rho_{skeletal}$ (g/cm^3)	V_p (cm^3/g)	ε	ε_b	S_{BET} (m^2/g)	d_{pore} (nm)	$V_{p,BET}$ (cm^3/g)
1.5Cu-Alg	5.0 ± 0.1	0.043	1.79	22.70	0.976	0.43 ± 0.01	572.96	36.86	5.202
1.5Ca-Alg	4.5 ± 0.1	0.056	1.82	17.31	0 .969	0.43 ± 0.01	449.72	11.63	1.102
1.5Zn-Alg	4.2 ± 0.1	0.065	1.87	14.83	0.965	0.41 ± 0.01	236.34	19.39	0.888
1.5Co-Alg	3.2 ± 0.1	0.151	1.77	6.06	0.915	0.40 ± 0.01	163.09	24.88	0.772
1.5Ni-Alg	3.1 ± 0.1	0.161	1.78	5.65	0.910	0.38 ± 0.01	169.2	28.6	0.789
1.5Mn-Alg	2.8 ± 0.1	0.191	1.89	4.71	0.899	0.30 ± 0.01	64.87	21.82	0.259
3Ca-Alg-Low	5.2 ± 0.2	0.05	1.85	19.46	0.973	0.41 ± 0.01	236.77	14.50	0.586
5Ca-Alg-Low	5.8 ± 0.2	0.075	1.77	12.77	0.958	0.45 ± 0.01	266.45	18.90	0.919
10Ca-Alg-Low	5.8 ± 0.2	0.137	1.84	6.76	0.926	0.45 ± 0.01	262.98	37.32	2.363

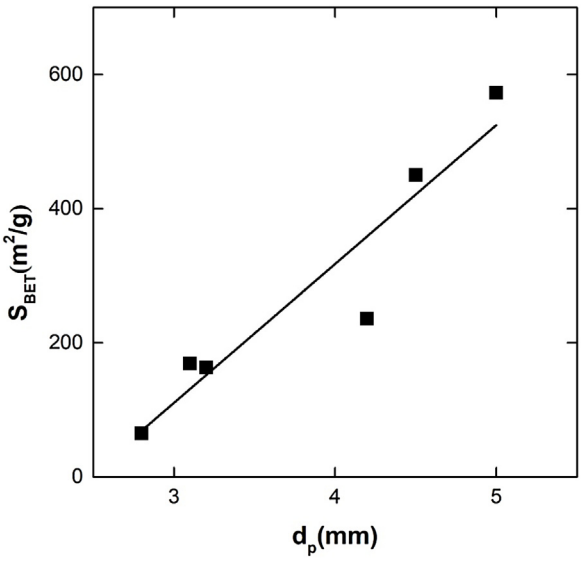

Fig. 2. BET surface area versus the particle diameter of various ionotropic aerogels prepared using 1.5 wt. % alginate solution (medium viscosity).

change after N_2 physisorption experiments and the determination of the equilibration point by the instrument during N_2 physisorption analysis was accurate, the most probable cause of this discrepancy can be considered as the presence of macropores. Moreover, decrease of both BET surface area and the pore volume calculated from physisorption data with the increasing degree of shrinkage implies the loss of mesopores in addition to macropores upon shrinkage resulting from weak interactions between the alginate and the cation. Interestingly, the BET surface area was found to be directly proportional to the particle diameter as indicated in Fig. 2.

In the case of Ca-alginate aerogels prepared using low viscosity alginate solution, the particle diameter increased from 5.2 mm to 5.8 mm when the concentration of the alginate was increased from 3 wt. % to 5 wt.%. Further increase of the alginate concentration did not affect aerogel's particle diameter. The decrease in gel shrinkage and the increase of the particle diameter implies that gel network becomes stronger when concentration of the alginate is higher. The effect of changing alginate concentration on BET surface area was similar to the effect on particle diameter. Both of them increased about 12% when the alginate concentration was increased from 3 wt. % to 5 wt. %. The pore volume calculated from physisorption data was directly proportional to the average pore diameter.

3.2. Supercritical drying of ionotropic alginate gels

Supercritical drying experiments for different ionotropic gels were carried out at 318 K and 100 bar with an exit CO_2 flow rate of 2 L/min at standard conditions. The packed bed volume of the alcogel particles in the drying vessel was 20 cm^3 for all alcogels except for 1.5Mn-Alg for which the packed bed volume was 15 cm^3.

Fig. 3 shows the concentration ethanol in the exit stream as a function time for the investigated ionotropic alginate alcogels. Cu and Ca-alginate gels dried slower than Zn, Mn and Co-alginate gels. Ni-alginate alcogels, on the other hand, initially dried slower than all of other alcogels. Drying times of ionotropic alcogels ranged between 15–25 min. Selmer et. al. reported the experimental drying curves for silica alcogel particles (diameter = 6.35 mm, porosity = 0.90 and tortuosity = 3.48) at 100 bar and 321 K using a cylindrical extractor (diameter = 0.017 m, volume = 151.4 ml) with a flow rate of 11.2 L/min at standard conditions. The drying time for this experiment was around 40 min. This value is in agreement with the data presented here considering that silica particles had larger

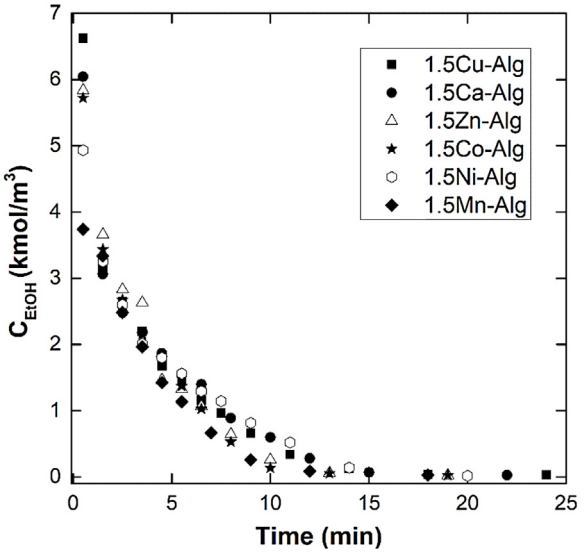

Fig. 3. Concentration ethanol in the exit stream as a function time for various ionotropic alginate alcogels at 318 K and 100 bar with a $scCO_2$ flow rate of 2 L/min at standard conditions.

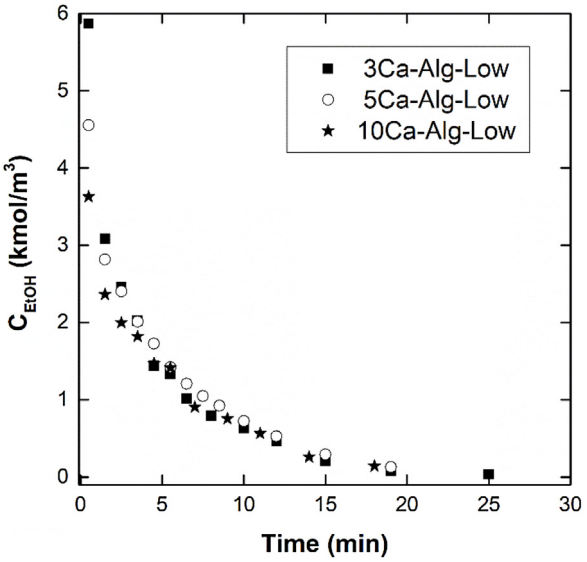

Fig. 5. Concentration ethanol in the exit stream as a function time for Ca-alginate (prepared using low viscosity solution) samples at 318 K and 100 bar with an exit CO_2 flow rate of 2 L/min at standard conditions.

diameters, which will increase the diffusion path length, therefore, drying time.

The drying behavior shown in Fig. 3 indicates a complex interplay between particle size, bed porosity and particle porosity. We recently showed that decreasing the particle size of Ca-alginate alcogels significantly reduced their drying time due to the decrease of diffusion path length [21]. So, the particle size and drying time are proportional. The bed porosity decreases with decreasing particle size. The bed porosity also influences interstitial velocity (the lower the bed porosity, the higher the interstitial velocity at constant volumetric flow rate). As another parameter, particle porosity also affects the drying kinetics. Decreasing the particle porosity slows down the diffusion of ethanol to the surface of the particle since the pore network becomes more tortuous. Thus, while the diffusion path length decreases with decreasing particle diameter, effective diffusivity of ethanol decreases due to a more tortuous pore network. Therefore, the effects of gel properties on the drying behavior is rather complex requiring simultaneous consideration of particle size, bed porosity and particle porosity. The use of reliable theoretical models can be beneficial for this purpose.

The effect of changing flow rate of $scCO_2$ on the drying kinetics of 1.5Cu-Alg and 1.5Co-Alg samples was studied by performing drying experiments at 318 K and 100 bar with an exit CO_2 flow rate of 2–4 L/min at standard conditions. Increase of flow rate from 2 L/min to 3 L/min led to faster drying times for both samples as shown in Fig. 4. For 1.5Cu-Alg, further increase of $scCO_2$ flow rate did not affect the drying curve.

3.3. Supercritical drying of Ca-alginate aerogels prepared using low viscosity alginate

Supercritical drying experiments were carried out at 318 K and 100 bar with an exit CO_2 flow rate of 2 L/min at standard conditions. The packed volume of the Ca-alginate particles in the drying vessel was 20 cm^3. The effect of changing temperature on the drying kinetics of 10Ca-Alg-Low was also investigated.

Drying curves in Fig. 5 show that initial rate of ethanol removal for 3Ca-Alg-Low was higher than those of 5Ca-Alg-Low and 10Ca-Alg-Low. This can be attributed to the smaller particle size of 3Ca-Alg-Low. However, after 10th minute of drying, all three curves became almost identical. The drying curves of 5Ca-Alg and 10Ca-Alg-Low were very similar to each other throughout the whole drying period although the initial rate of ethanol removal was slightly higher for 5Ca-Alg-Low. For these three samples, particle porosity decreased with increasing alginate concentration. Thus,

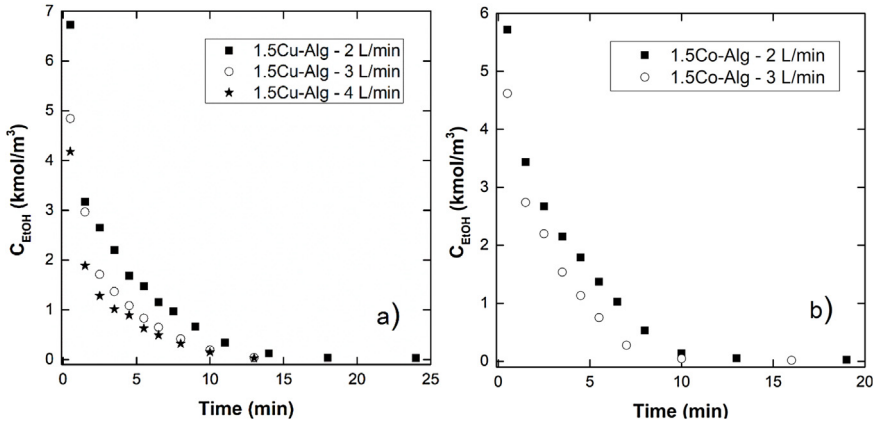

Fig. 4. Concentration ethanol in the exit stream as a function time for **(a)** 1.5Cu-Alg at 318 K and 100 bar with an exit CO_2 flow rate of 2–4 L/min at standard conditions, **(b)** 1.5Co-Alg at 318 K and 100 bar with an exit CO_2 flow rate of 2–3 L/min at standard conditions.

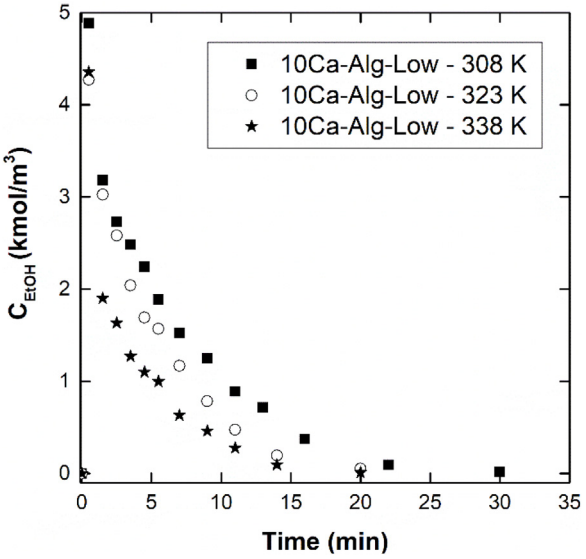

Fig. 6. Concentration ethanol in the exit stream as a function time for 10Ca-Alg-Low at 308, 323 and 338 K and 120 bar with a $scCO_2$ flow rate of 2 L/min at standard conditions.

for this set of samples the influence of particle size on drying kinetics is more pronounced than the influence of particle porosity.

Experiments were carried out at three different temperatures of 308, 323, and 338 K at 120 bar with an exit CO_2 flow rate of 2 L/min at standard conditions in order to investigate the effect of temperature on the drying kinetics of 10Ca-Alg-Low gel particles. Increasing temperature led to shorter drying times as is illustrated in Fig. 6. The effect of increasing temperature from 308 K to 323 K on the drying behavior was more significant than further increasing the temperature from 323 K to 338 K.

3.4. Modeling of supercritical drying

The partial differential equation describing mass transfer of ethanol inside a spherical gel particle is given by;

$$\frac{\partial C_s}{\partial t} = \frac{1}{r^2}\frac{\partial}{\partial r}\left(r^2 D_e \frac{\partial C_s}{\partial r}\right) \tag{7}$$

where C_s is concentration of ethanol inside the gel, D_e is effective diffusion coefficient of ethanol, t is time, and r is the radial position at which the diffusion occurs inside the gel.

The initial condition and the boundary conditions for Eq. (7) are:

$$t = 0\,, \quad C_s = C_{s0} \tag{8}$$

$$r = 0, \quad \frac{\partial C_s}{\partial r} = 0 \tag{9}$$

$$r = R\,, \quad D_e \frac{\partial C_s}{\partial r} = k_f (C_f - C_{sR}) \tag{10}$$

where C_f is concentration of ethanol in the flowing fluid outside the particles, R is the radius of the gel particle, C_{sR} is the concentration of the ethanol at the surface of the gel particle, that is $C_{sR} = C_s$ at $r = R$.

Initially, there was pure ethanol inside the gel (Eq. 8). Symmetry boundary condition at the center of the spherical particle was implemented as shown in Eqs. (9 and 10) indicates that there is convective mass transfer from the surface of the gel particles ($r = R$) into the flowing fluid stream governed by the mass transfer coefficient k_f.

Table 2
Summary of the conditions for drying experiments performed with ionotropic alginate alcogels.

Exp. No.	Sample Name	Temperature (K)	Pressure (bar)	Q_{CO2} (L/min)
1	1.5Cu-Alg	318	100	2
2	1.5Ca-Alg	318	100	2
3	1.5Zn-Alg	318	100	2
4	1.5Co-Alg	318	100	2
5	1.5Ni-Alg	318	100	2
6	1.5Mn-Alg	318	100	2
7	1.5Cu-Alg	318	100	3
8	1.5Cu-Alg	318	100	4
9	1.5Co-Alg	318	100	3

The partial differential equation obtained from a mass balance in a differential volume element in the fluid outside the gel particles is given by;

$$\frac{\partial C_f}{\partial t} = D_L \frac{\partial^2 C_f}{\partial z^2} - u_0 \frac{\partial C_f}{\partial z} - \frac{3(1-\varepsilon_b)}{\varepsilon_b}\frac{1}{R} k_f \left(C_f - C_{fR}\right) \tag{11}$$

where $C_{fR} = C_{sR}$, D_L is axial dispersion coefficient of ethanol, ε_b is the porosity of the packed bed, k_f is the external mass transfer coefficient and u_0 is the interstitial velocity of flowing fluid stream.

The initial condition and the boundary conditions for Eq. (11) were as follows;

$$t = 0\,, \; C_f = C_{f0} \tag{12}$$

$$z = 0, \; u_0 C_f - D_L \frac{\partial C_f}{\partial z} = 0 \tag{13}$$

$$z = L, \; \frac{\partial C_f}{\partial z} = 0 \tag{14}$$

Initially, the pores of the gel and the void volume of the extraction vessel were filled with pure ethanol (Eq. 12). Danckwerts boundary condition was implemented for the flowing fluid at the top of the drying vessel, $z = 0$, indicating the dispersion of ethanol is counterbalanced by the convective term to prevent ethanol loss (Eq. 13). Concentration of ethanol at the exit of the vessel ($z = L$) did not change with position (Eq. 14).

The model assumes that the process is isothermal and isobaric. A radially symmetric concentration distribution of ethanol was also assumed. Since the change in particle diameter is very small during supercritical drying, the bed porosity and bed length was considered to be constant. Moreover, since the particles were closely and uniformly packed, channeling and bed compression were assumed not to be present in the vessel. The possible spillover of ethanol due to the volume expansion by CO_2 was not considered in constructing the model. The density and viscosity of the fluid around the gel particles were taken as those of pure CO_2. This assumption would not be valid for the initial stages of drying where the mole fraction of ethanol is high. This stage made up only 10–15 % of total drying time. Besides, the main mode of mass transport in this period would be the convective mass transport from the particle surface, which was considered in the model using a developed dimensionless number correlation to calculate the mass transfer coefficients.

Numerical method of lines (NMOL) was implemented by converting the coupled partial differential equations, Eqs. (7 and 11), into a coupled set of differential-algebraic equations by discretizing only the spatial dimension via finite difference method. The temporal dimension, t was allowed to be continuous. Then, an available built-in ordinary differential equation (ODE) solver in MATLAB was utilized to solve the ODEs obtained from discretization. The model calculates concentration of ethanol in the fluid phase inside the particles, C_s, as a function of r, z and t, and concentration of ethanol in the fluid phase flowing around the particles, C_f, as a function of z

Table 3
Summary of the conditions and gel properties for drying experiments performed with Ca-alginate aerogels prepared using low viscosity alginate solution.

Exp. No.	Sample Name	Temperature (K)	Pressure (bar)	Q_{CO2} (L/min)
1	3Ca-Alg-Low	318	100	2
2	5Ca-Alg-Low	318	100	2
3	10Ca-Alg-Low	318	100	2
4	10Ca-Alg-Low	308	120	2
5	10Ca-Alg-Low	323	120	2
6	10Ca-Alg-Low	338	120	2

Table 4
Summary of the parameter estimation for mathematical modeling.

Parameter	Value	References
Tortuosity, τ	$1/\varepsilon$	[38]
Density & viscosity	Varies with T, P	[39]
Effective diffusion coefficient, D_e	$D_e = D_{og}^{(1-x_{co_2})} \times D_{ol}^{x_{co_2}} \times \varepsilon/\tau$	[40]
Binary diffusion coefficient of ethanol in $scCO_2$ at infinite dilution, D_{og}	$D_{og} = T \times (-9.434 \times 10^{-7}\rho_{CO_2} + 1.296 \times 10^{-6})$	[41]
Binary diffusion coefficient of $scCO_2$ in ethanol at infinite dilution, D_{ol}	$D_{ol} = 336.5 \times 10^{-9} exp\left(\frac{-1314.7}{T}\right)$	[42]
Axial dispersion coefficient, D_L	$D_L = \frac{u_0 \times d_p}{Pe}$, $Pe = 1.634Re^{0.265}Sc^{-0.919}$, $Re = \frac{d_p u_0 \varepsilon_b \rho_{CO_2}}{\mu_{CO_2}}$, $Sc = \frac{\mu_{CO_2}}{\rho_{CO_2} D_{og}}$	[43]
Mass transfer coefficient, k_f	$k_f = \frac{Sh \times D_{og}}{d_p}$, $Sh = 0.249Re^{0.295}Sc^{0.333}$	[21]

Table 5
Physicochemical properties of CO_2 and calculated transport coefficients and dimensionless numbers for the experiments listed in Table 2.

Exp. No.	ρ_{CO2} (kg/m^3)	μ_{CO2} (Pa.s)	D_{e-min} (m^2/s)	D_{e-max} (m^2/s)	*Re*	*Sc*	*Sh*	k_f (m/s)
1	498.3	3.603×10^{-5}	5.144×10^{-9}	2.185×10^{-8}	51.9	3.2	1.2	5.372×10^{-6}
2	498.3	3.603×10^{-5}	5.070×10^{-9}	2.153×10^{-8}	46.7	3.2	1.1	5.786×10^{-6}
3	498.3	3.603×10^{-5}	5.029×10^{-9}	2.136×10^{-8}	43.6	3.2	1.1	6.074×10^{-6}
4	498.3	3.603×10^{-5}	4.521×10^{-9}	1.920×10^{-8}	33.2	3.2	1.0	7.358×10^{-6}
5	498.3	3.603×10^{-5}	4.472×10^{-9}	1.899×10^{-8}	32.2	3.2	1.0	7.254×10^{-6}
6	498.3	3.603×10^{-5}	3.363×10^{-9}	1.854×10^{-8}	29.1	3.2	1.0	8.084×10^{-6}
7	498.3	3.603×10^{-5}	5.144×10^{-9}	2.185×10^{-8}	77.9	3.2	1.3	6.054×10^{-6}
8	498.3	3.603×10^{-5}	5.144×10^{-9}	2.185×10^{-8}	103.9	3.2	1.4	6.590×10^{-6}
9	498.3	3.603×10^{-5}	4.521×10^{-9}	1.920×10^{-8}	49.9	3.2	1.2	8.293×10^{-6}

Table 6
Physicochemical properties of CO_2 and calculated transport coefficients and transport coefficients for the experiments listed in Table 3.

Exp. No.	ρ_{CO2} (kg/m^3)	μ_{CO2} (Pa.s)	D_{e-min} (m^2/s)	D_{e-max} (m^2/s)	*Re*	*Sc*	*Sh*	k_f (m/s)
1	498.3	3.603×10^{-5}	5.112×10^{-9}	2.172×10^{-8}	54.0	3.2	1.2	5.225×10^{-6}
2	498.3	3.603×10^{-5}	4.956×10^{-9}	2.105×10^{-8}	60.2	3.2	1.2	4.838×10^{-6}
3	498.3	3.603×10^{-5}	4.630×10^{-9}	1.967×10^{-8}	60.2	3.2	1.2	4.838×10^{-6}
4	767.1	6.552×10^{-5}	4.049×10^{-9}	1.900×10^{-8}	33.1	4.0	1.1	4.226×10^{-6}
5	584.7	4.380×10^{-5}	4.936×10^{-9}	2.376×10^{-8}	49.6	2.7	1.1	5.243×10^{-6}
6	382.9	2.899×10^{-5}	5.913×10^{-9}	2.988×10^{-8}	74.9	2.2	1.2	6.925×10^{-6}

and t. The inlet volumetric flow rate of CO_2 at extraction conditions was varied as a function of time in solving model equations and it was taken as the sum of the volumetric flow rate of ethanol and CO_2 at the exit of the bed at extraction conditions. The inlet volumetric flow rates of CO_2 as a function of time for all of the experiments can be found in Table S3 and S4 of the Supplementary Information. Parameters in the model were obtained from data or correlations in the literature as shown in Table 4.

Table 5 and 6 show the physicochemical properties of CO_2, calculated transport coefficients and dimensionless numbers for the performed experiments. Minimum and maximum values of effective diffusion coefficients were also listed. Effective diffusion coefficient increased with increasing particle porosity, and in this case with increasing particle diameter, for a constant temperature and pressure. Mass transfer coefficient increased with decreasing particle diameter. Moreover, increase in temperature led to increase of both diffusion coefficients and mass transfer coefficients for a constant particle diameter and porosity.

Calculated mass transfer coefficient for the experiment with 1.5Cu-Alg at 318 K and 100 bar with an exit CO_2 flow rate of 2 L/min at standard conditions was compared with the mass transfer coefficients calculated using the correlations in the literature in Table 7. There is one order of magnitude difference between the literature values and the estimated value in this study.

3.4.1. Comparison of experimental data and model predictions

Table 2 show the summary of the operating conditions for the experiments performed with ionotropic gel particles. Simulations were performed using the proposed model to calculate the fraction of the ethanol in the gel removed from the gel particles during

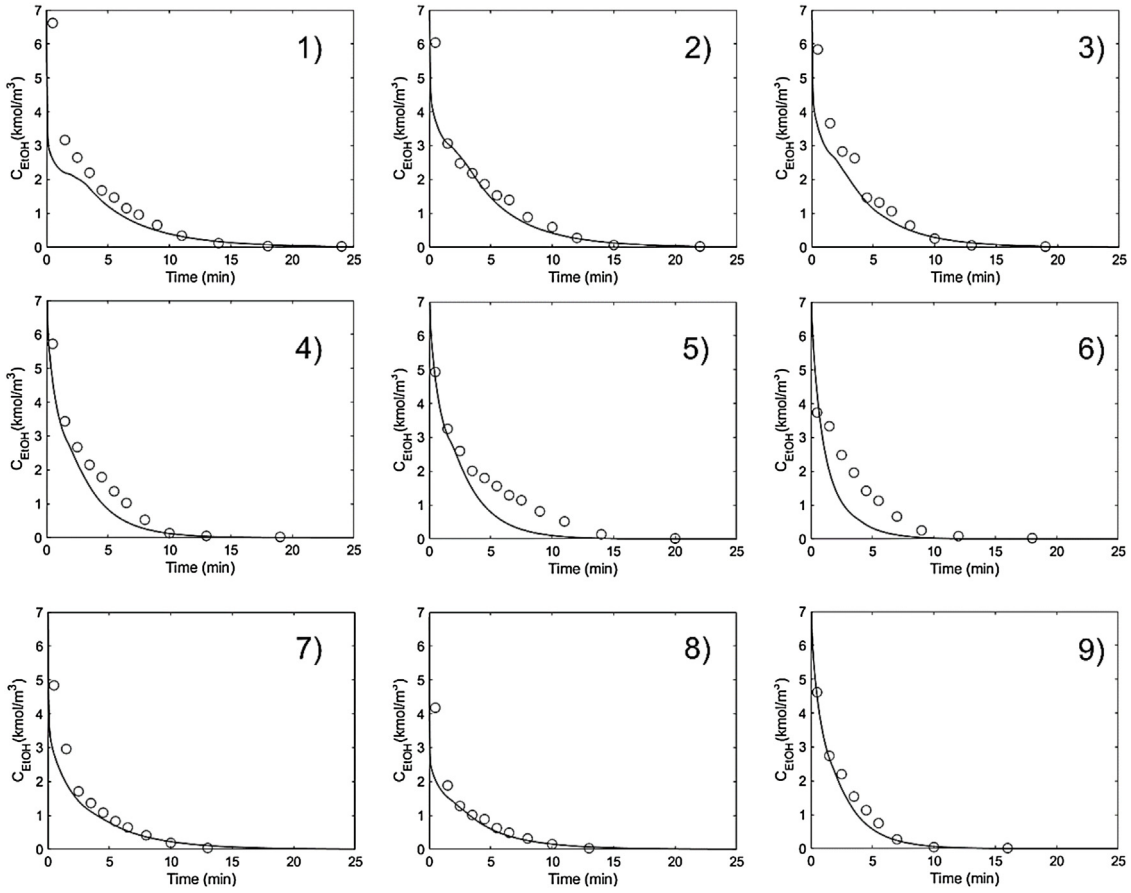

Fig. 7. Comparison of the ethanol concentrations in the exit stream versus time estimated by the model with the experimental data for the experiments listed in Table 2. Solid curves indicate the model results whereas empty circles show the experimental data points. Numbers corresponds to experiment numbers denoted in Table 2.

supercritical drying. Fig. 7 shows the comparison of the ethanol concentration in the exit stream between the model results and the experimental data. Comparisons with respect to fraction of ethanol removed can be found in Figure S1 of Supplementary Information.

The performance of the proposed model in predicting the experimental data of alginate aerogels with different properties was very good. The predicted drying behavior of experiments 5 and 6 were slightly slower than the experimental profiles. On the other hand, the model is capable of accounting for the effect of changing flow rates of $scCO_2$ on the drying profiles for Cu and Co-alginate alcogels. This indicates that our previously proposed correlation to calculate mass transfer coefficients can be utilized for gels with different particle diameter and porosity.

The model does not consider any interactions between the solid backbone of the gel particles and ethanol. Therefore, the changes in drying profiles with different ionotropic gels can be attributed solely to the change in diameter and porosity of the particles since the model predicts these changes well. This might be expected if one considers that the effect of changing the chemistry of the solid backbone of the gel particles would only affect the adsorption strength of ethanol in the form of an adsorbed layer to the solid backbone. For ionotropic gels investigated in this study, the amount of ethanol in the adsorbed layer is very small compared to the amount of liquid ethanol inside the pores. This adsorbed fraction may need to be considered for gels which have low pore volumes and high surface areas.

Another important consideration may be the change of the pore structure of the gel with different cations as shown by Agulhon et al. for Cu, Ca, Co, and Mn-alginate aerogels due to the different ratios of the mannuronic/guluronic residues of the alginate [44]. Actually, each ionotropic alginate aerogel had a different average pore size, pore size distribution, BET surface area and porosity. On the other hand, in the presented model, the effective diffusivity of ethanol in the pores is estimated by using solely the porosity information from particle density irrespective of the values of pore diameter and pore size distributions.

Table 7
Comparison of the mass transfer coefficients estimated using the developed correlation and correlations from the literature for the experiment with 1.5Cu-Alg at 318 K and 100 bar with an exit CO_2 flow rate of 2 L/min at standard conditions.

Sherwood number correlation	k_f (m/s)
$Sh = 0.249Re^{0.295}Sc^{0.333}$ [21]	5.372×10^{-6}
$Sh = 2.1 + 1.1Re^{0.6}Sc^{0.333}$ [17]	8.834×10^{-5}
$Sh = 0.206Re^{0.8}Sc^{0.333}$ [16]	3.266×10^{-5}
$Sh = 0.269Re^{0.83}Sc^{0.333}$ [15]	4.802×10^{-5}
$Sh = 0.38Re^{0.83}Sc^{0.333}$ [20]	6.783×10^{-5}

Summary of the operating conditions of supercritical drying of low viscosity Ca-alginate alcogel particles are listed in Table 3. A good agreement between the ethanol concentrations in the exit stream estimated by the model and the experimental data is obtained as shown in Fig. 8. Comparison of the fraction of ethanol removal curves estimated by the model with the experimental data can be found in Figure S2 of Supplementary Information. The model was responsive to the changes in drying temperature for 10Ca-Alg-Low samples. Again, the model can predict the drying profiles from particle size and porosity information with no further input about the material properties.

A simulation was also performed using the presented model for silica alcogels particles dried (diameter=6.35 mm, poros-

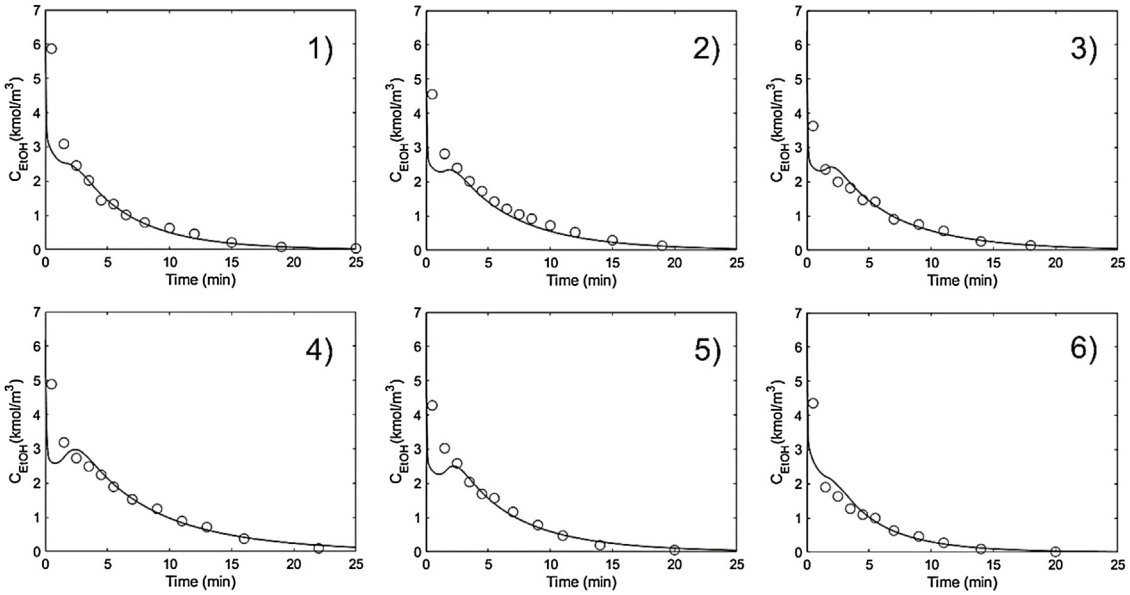

Fig. 8. Comparison of the ethanol concentrations in the exit stream versus time estimated by the model with the experimental data for the experiments listed in Table 3. Solid curves indicate the model results whereas empty circles show the experimental data points. Numbers corresponds to experiment numbers denoted in Table 3.

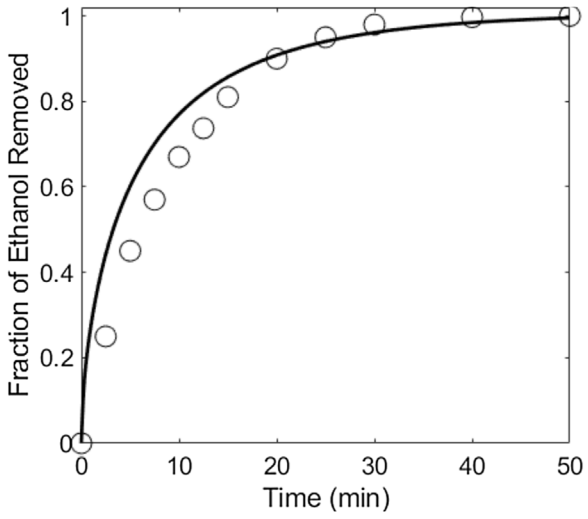

Fig. 9. Comparison of the fraction of ethanol removed from silica alcogel particles versus time [14] estimated by our model with the experimental data. Solid curves indicate the model results whereas empty circles show the experimental data points.

ity = 0.90 and tortuosity = 3.48) at 100 bar and 321 K inside a cylindrical extractor (diameter = 0.017 m, volume = 151.4 ml, bed porosity = 0.6) with a flow rate of 11.2 L/min at standard conditions [14]. Fig. 9 shows that our model could successfully predict the drying time and profile reported in the literature which was around 40 min.

4. Conclusions

The kinetics of supercritical drying of a series of M-alginate (M = Ca^{2+}, Mn^{2+}, Ni^{2+}, Co^{2+}, Cu^{2+} and Zn^{2+}) gel particles was investigated. The data indicated a high removal rate initially followed by a diminishing rate as time progressed. A model consisting of coupled partial differential equations describing mass transport of ethanol in the fluid inside the gel particles and in the flowing fluid around gel particles was found to predict the experimental drying profiles, including the high initial rates of removal, successfully. The good agreement suggests that the mass transfer correlation previously developed for drying of Ca-alginate particles is also valid for other M-alginate particles investigated in this study [21]. Moreover, it was seen that the changes in the drying kinetics for different types of gels could be attributed only to the changes in the physical parameters such as particle diameter and porosity of the particles rather than the surface chemistry of the gel. Further studies with other types of organic and inorganic gel particles would be beneficial to extend this model to all types of gel particles.

Acknowledgements

This work was supported by European Unionś Horizon 2020 research and innovation programme under grant agreement No: 685648.

Appendix A. Supplementary data

Supplementary material related to this article can be found, in the online version, at doi:https://doi.org/10.1016/j.supflu.2019.104571.

References

[1] M.A. Aegerter, N. Leventis, M.M. Koebel, Aerogels Handbook, Springer, New York, 2011 https://books.google.com.tr/books?id=3FXWzJFOlnAC.
[2] S. Zheng, X. Hu, A.-R. Ibrahim, D. Tang, Y. Tan, J. Li, Supercritical fluid drying: classification and applications, Recent Patents Chem. Eng. 3 (2011) 230–244, http://dx.doi.org/10.2174/1874478811003030230.
[3] K.I. Jensen, J.M. Schultz, F.H. Kristiansen, Development of windows based on highly insulating aerogel glazings, J. Non. Solids 350 (2004) 351–357, http://dx.doi.org/10.1016/j.jnoncrysol.2004.06.047.
[4] C. Buratti, E. Moretti, Glazing systems with silica aerogel for energy savings in buildings, Appl. Energy 98 (2012) 396–403, http://dx.doi.org/10.1016/j.apenergy.2012.03.062.
[5] E. Elaloui, P. Achard, B. Chevalier, J.-L. Chevalier, M. Durant, G.M. Pajonk, Improved Monolithic Aerogel for Transparent Glass Spacer in Innovative Windows, 1992, pp. 1711–1727, http://dx.doi.org/10.1117/12.130528.
[6] New Spaceloft® Insul-Cap™ From Aspen Aerogels Improves Thermal Efficiency of Wall Framing, 2007 (accessed September 12, 2017) http://news.aerogel.com/press-releases?item=66347.
[7] K. Ganesan, T. Budtova, L. Ratke, P. Gurikov, V. Baudron, I. Preibisch, P. Niemeyer, I. Smirnova, B. Milow, Review on the production of polysaccharide aerogel particles, Materials (Basel). 11 (2018) 2144.
[8] Z. Ulker, C. Erkey, An emerging platform for drug delivery: aerogel based systems, J. Control. Release 177 (2014) 51–63, http://dx.doi.org/10.1016/j.jconrel.2013.12.033.

[9] C. Moreno-Castilla, F.J. Maldonado-Hódar, Carbon aerogels for catalysis applications: an overview, Carbon 43 (2005) 455–465, http://dx.doi.org/10.1016/j.carbon.2004.10.022.
[10] J. Stergar, U. Maver, Review of aerogel-based materials in biomedical applications, J. Solgel Sci. Technol. 77 (2016) 738–752, http://dx.doi.org/10.1007/s10971-016-3968-5.
[11] DOWSILTM VM-2270 Aerogel Fine Particles, (n.d.).https://consumer.dow.com/en-us/pdp.dowsilTMvm-2270aerogelfineparticles.04060829z.html?tab=overview&id=04060829z (accessed September 12, 2018).
[12] İ. Şahin, Y. Özbakır, Z. İnönü, Z. Ulker, C. Erkey, Kinetics of Supercritical Drying of Gels, Gels 4 (2018), http://dx.doi.org/10.3390/gels4010003.
[13] I. Selmer, A.S. Behnecke, J. Quiño, A.S. Braeuer, P. Gurikov, I. Smirnova, Model development for sc-drying kinetics of aerogels: Part 1. Monoliths and single particles, J. Supercrit. Fluids 140 (2018) 415–430, http://dx.doi.org/10.1016/j.supflu.2018.07.002.
[14] I. Selmer, A.-S. Behnecke, P. Farrell, A.B. Morales, P. Gurikov, I. Smirnova, Model development for sc-drying kinetics of aerogels: Part 2. Packed bed of spherical particles, J. Supercrit. Fluids (2018), http://dx.doi.org/10.1016/j.supflu.2018.07.006.
[15] F. Stüber, A.M. Vazquez, M.A. Larrayoz, F. Recasens, Supercritical fluid extraction of packed beds : external mass transfer in Upflow and downflow operation, Ind. Eng. Chem. Res. 35 (1996) 3618–3628, http://dx.doi.org/10.1021/ie9601514.
[16] J. Puiggené, M.A. Larrayoz, F. Recasens, Free liquid-to-supercritical fluid mass transfer in packed beds, Chem. Eng. Sci. 52 (1997) 195–212, http://dx.doi.org/10.1016/S0009-2509(96)00379-X.
[17] N. Wakao, S. Kagei, Heat and Mass Transfer in Packed Beds, Gordon and Breach Science Publishers, 1982 https://books.google.com.tr/books?id=Ya5hzOgC05wC.
[18] S. Zheng, X. Hu, A.-R. Ibrahim, D. Tang, Y. Tan, J. Li, Supercritical fluid drying: classification and applications, Recent Patents Chem. Eng. 3 (2010) 230–244, http://dx.doi.org/10.2174/2211334711003030230.
[19] Z. Huang, X. Shi, W. Jiang, Theoretical models for supercritical fluid extraction, J. Chromatogr. A 1250 (2012) 2–26, http://dx.doi.org/10.1016/j.chroma.2012.04.032.
[20] C.-S. Tan, S.-K. Liang, D.-C. Liou, Fluid—solid mass transfer in a supercritical fluid extractor, Chem. Eng. J. 38 (1988) 17–22, http://dx.doi.org/10.1016/0300-9467(88)80049-2.
[21] İ. Şahin, E. Uzunlar, C. Erkey, Investigation of kinetics of supercritical drying of alginate alcogel particles, J. Supercrit, Fluids 146 (2019) 78–88, http://dx.doi.org/10.1016/j.supflu.2018.12.019.
[22] Y. Özbakir, C. Erkey, Experimental and theoretical investigation of supercritical drying of silica alcogels, J. Supercrit. Fluids 98 (2015) 153–166, http://dx.doi.org/10.1016/j.supflu.2014.12.001.
[23] S. Wang, T. Vincent, C. Faur, E. Guibal, Alginate and algal-based beads for the sorption of metal cations: Cu(II) and Pb(II), Int. J. Mol. Sci. 17 (2016) 1453, http://dx.doi.org/10.3390/ijms17091453.
[24] P. Agulhon, S. Constant, B. Chiche, L. Lartigue, J. Larionova, F. Di Renzo, F. Quignard, Controlled synthesis from alginate gels of cobalt–manganese mixed oxide nanocrystals with peculiar magnetic properties, Catal. Today 189 (2012) 49–54, http://dx.doi.org/10.1016/j.cattod.2012.03.052.
[25] Ý.A. Mørch, I. Sandvig, Ø. Olsen, I. Donati, M. Thuen, G. Skjåk-Bræk, O. Haraldseth, C. Brekken, Mn-alginate gels as a novel system for controlled release of Mn2+ in manganese-enhanced MRI, Contrast Media Mol. Imaging 7 (2012) 265–275, http://dx.doi.org/10.1002/cmmi.493.
[26] R.R. Escudero, M. Robitzer, F. Di Renzo, F. Quignard, Alginate aerogels as adsorbents of polar molecules from liquid hydrocarbons: hexanol as probe molecule, Carbohydr. Polym. 75 (2009) 52–57, http://dx.doi.org/10.1016/j.carbpol.2008.06.008.
[27] X. Sun, X. Zhu, X. Yang, J. Sun, Y. Xia, D. Yang, CoFe2O4/carbon nanotube aerogels as high performance anodes for lithium ion batteries, Green Energy Environ. 2 (2017) 160–167, http://dx.doi.org/10.1016/j.gee.2017.01.008.
[28] R. Horga, F. Di Renzo, F. Quignard, Ionotropic alginate aerogels as precursors of dispersed oxide phases, Appl. Catal. A Gen. 325 (2007) 251–255, http://dx.doi.org/10.1016/j.apcata.2007.02.042.
[29] A. Veronovski, Ž. Knez, Z. Novak, Preparation of multi-membrane alginate aerogels used for drug delivery, J. Supercrit. Fluids 79 (2013) 209–215, http://dx.doi.org/10.1016/j.supflu.2013.01.025.
[30] A. Haug, J. Bjerrum, O. Buchardt, G.E. Olsen, C. Pedersen, J. Toft, The affinity of some divalent metals for different types of alginates, Acta Chem. Scand. 15 (1961) 1794–1795, http://dx.doi.org/10.3891/acta.chem.scand.15-1794.
[31] A. Haug, O. Smidsrød, B. Högdahl, H.A. Øye, S.E. Rasmussen, E. Sunde, N.A. Sørensen, Selectivity of some anionic polymers for divalent metal ions, Acta Chem. Scand. 24 (1970) 843–854, http://dx.doi.org/10.3891/acta.chem.scand.24-0843.
[32] J. Van Keulen, Density of porous solids, Matériaux Constr. 6 (1973) 181–183, http://dx.doi.org/10.1007/BF02479031.
[33] W.B. Innes, Total porosity and particle density of fluid catalysts by liquid titration, Anal. Chem. 28 (1956) 332–334, http://dx.doi.org/10.1021/ac60111a013.
[34] D. Huang, C. Guo, M. Zhang, L. Shi, Characteristics of nanoporous silica aerogel under high temperature from 950°C to 1200°C, Mater. Des. 129 (2017) 82–90, http://dx.doi.org/10.1016/j.matdes.2017.05.024.
[35] A.R. Yaqubzadeh, A. Ahmadpour, T.R. Bastami, M.R. Hataminia, Low-cost preparation of silica aerogel for optimized adsorptive removal of naphthalene from aqueous solution with central composite design (CCD), J. Non. Solids 447 (2016) 307–314, http://dx.doi.org/10.1016/j.jnoncrysol.2016.06.022.
[36] K. Hindelang, T. Gottschalk-Gaudig, D. Jantke, R. Weidner, Process for Producing Organically Modified Aerogels, 2018.
[37] G. Reichenauer, G.W. Scherer, Effects upon nitrogen sorption analysis in aerogels, J. Colloid Interface Sci. 236 (2001) 385–386, http://dx.doi.org/10.1006/jcis.2000.7419.
[38] N. Wakao, J.M. Smith, Diffusion in catalyst pellets, Chem. Eng. Sci. 17 (1962) 825–834, http://dx.doi.org/10.1016/0009-2509(62)87015-8.
[39] E. Shen, V.K. Siderius, D.W. Krekelberg, W.P, H.W. Hatch, NIST Standard Reference Simulation Website, NIST Stand. Ref. Database Number 173, 2018, http://dx.doi.org/10.18434/T4M88Q (accessed June 20, 2018).
[40] A. Vignes, Diffusion in binary solutions: variation of diffusion coefficient with composition, Ind. Eng. Chem. Fundam. 5 (1966) 189–199, http://dx.doi.org/10.1021/i160018a007.
[41] A.L. Magalhães, P.F. Lito, F.A. Da Silva, C.M. Silva, Simple and accurate correlations for diffusion coefficients of solutes in liquids and supercritical fluids over wide ranges of temperature and density, J. Supercrit. Fluids 76 (2013) 94–114, http://dx.doi.org/10.1016/j.supflu.2013.02.002.
[42] E.D. Snijder, M.J.M. Te Riele, G.F. Versteeg, W.P.M. Van Swaaij, Diffusion coefficients of CO, COS, N20, and N2 in ethanol and toluene, J. Chem. Eng. Data 40 (1996) 37–39, http://dx.doi.org/10.1021/je00017a010.
[43] C.-S. Tan, D.-C. Liou, Axial dispersion of supercritical carbon dioxide in packed beds, Ind. Eng. Chem. Res. 28 (1989) 1246–1250, http://dx.doi.org/10.1021/ie00092a020.
[44] P. Agulhon, M. Robitzer, L. David, F. Quignard, Structural regime identification in ionotropic alginate gels: influence of the cation nature and alginate structure, Biomacromolecules. 13 (2012) 215–220, http://dx.doi.org/10.1021/bm201477g.